

Vibrational, Electronic and Structural Study of Sprayed ZnO Thin Film Based on the IR-Raman Spectra and DFT Calculations

Bechir Ouni*, Tarek Larbi, Mosbah Amlouk

Unité de Physique des Dispositifs à Semi-Conducteurs, Faculté des Sciences de Tunis, Tunis El Manar University, Tunis, Tunisia
Email: *bachir.ouni@laposte.net

How to cite this paper: Ouni, B., Larbi, T. and Amlouk, M. (2022) Vibrational, Electronic and Structural Study of Sprayed ZnO Thin Film Based on the IR-Raman Spectra and DFT Calculations. *Crystal Structure Theory and Applications*, 11, 23-38.
<https://doi.org/10.4236/csta.2022.112002>

Received: April 16, 2022

Accepted: May 28, 2022

Published: May 31, 2022

Copyright © 2022 by author(s) and Scientific Research Publishing Inc.

This work is licensed under the Creative Commons Attribution International License (CC BY 4.0).

<http://creativecommons.org/licenses/by/4.0/>



Open Access

Abstract

Applying the Density Function Theory (DFT) combined with LCAO basis set and employing the B3LYP hybrid functional, the optimized geometrical parameters, electronic properties, as well as the Infrared and Raman spectra for wurtzite-ZnO structure were investigated. Prior to computing, ZnO thin film prepared by the spray pyrolysis method is characterized by X-ray diffraction using Rietveld refinement. This analysis shows that ZnO has hexagonal wurtzite structure ($P6_3mc$) with lattice parameters, $a = 3.2467$ and $c = 5.2151$ Å in good agreement with our predicted optimized geometry. Atomic force microscopy (AFM), Raman spectroscopy and UV-Vis-NIR spectrophotometry techniques are used to explore morphological, optical and vibrational properties of the sprayed ZnO thin film. The computed band gap ($E_g^{DFT} = 3.35$ eV) is in excellent agreement with that deduced from UV-Vis transmission ($E_g^{Optic} = 3.3$ eV). The simulated infrared and Raman spectra were also calculated, and a good agreement with the measured spectra is obtained. Finally, a detailed interpretation of the infrared and Raman spectra is reported.

Keywords

DFT, Thin Film, Electronic Structure, IR and Raman Spectroscopy

1. Introduction

Zinc oxide (ZnO) continues to garner an extensive research interest owing to several of its promising applications. It has been the object of the renewed research for a wide range of applications such as light emitting diodes [1], laser diodes, gas sensor [2], thin film solar cells [3] and spintronics [4]. The interest of

ZnO resides especially in its wide direct band gap (3.4 eV), high n-type conductivity, high thermal conductivity and its large exciton binding (60 meV) [5]. Nevertheless, during the design, the control of structural defects as well as surface and interfacial structures is essential for optimizing the device performance [6]. In addition, it is noted that the growth conditions affect the band gap which is a key parameter in the design of optoelectronic devices.

Synthesis of ZnO thin films has been performed by several techniques, such as spray pyrolysis, sol-gel [7], pulsed laser deposition [8] RF magnetron sputtering [9] and Chemical Vapour Deposition [10]. The spray pyrolysis technique has been selected owing to its large deposition area, low cost process, and viable approach of producing good quality films. Thus, a lot of work have been carried out and various parameters of the deposition of ZnO films such as, substrate temperature, carrier gas flow rate, solution flow rate, nozzle to substrate distance and film thickness have been optimized [11] [12] [13] [14] [15].

Several studies have been done on the electronic structure of ZnO in the wurtzite phase using *ab initio* calculations [16] [17] [18] [19]. Due to the various functionals employed, the theoretical band gap values cover a wide spectrum. Franklin *et al.* reported that physical origin of the changes in the band gap may be related to the trial basis set which is utilized for iterative solutions of the Kohn-Sham equations [20]. Also, Arrigo *et al.* showed that the severe underestimation of the band gap, which is mainly due to a wrong energy position of the d-bands of the Zn atoms, leads to an inadequate description of vibrational and dielectric properties [21]. Bernasconi *et al.* showed that optical response properties, computed with the Coupled-Perturbed-Hartree-Fock/Kohn-Sham method with hybrid functionals, can reach an accuracy comparable to experimental estimates for various classes of semiconductors and oxides [22]. Moreover, IR and Raman spectroscopy can offer valuable information on structural changes, lattice defects, grain size, and the concentration of impurities presents in the ZnO host lattice [23]-[28]. Cheng *et al.* have reported that the lattice dynamics in ZnO is very sensitive to the compositional disorder which introduces changes in the electronic properties and vibrational phonons [29]. Indeed, in the wurtzite structure of ZnO, the E_2 phonon frequency can be affected by compressive stress, tensile stress, grain size, thickness of the film and mismatch of thermal expansion coefficients of the layer and the glass substrate [8]. Also, David *et al.* also reported that the E_2 Raman active phonon is systematically affected by the particle size [30].

As far as we know, there is not yet in the literature IR and Raman spectroscopy using quantum mechanical calculations of the ZnO have been reported in detail. In the present work, first principle DFT calculations using B3LYP hybrid functional have been performed to investigate structural and electronic properties as well as infrared and Raman spectra of wurtzite structured ZnO. Specifically, we report a combined experimental and theoretical analysis of sprayed ZnO thin film. We discuss below the features of calculation method for simulating the structural parameters, electronic band structure, Infrared (IR) and Ra-

man spectra that show a good agreement with our experimental data.

2. Films Preparation and Characterization Techniques

Zinc oxide thin films have been prepared on heated glass substrates at 460 °C by the spray pyrolysis technique. The starting solution is made up of Zinc acetate dihydrate ($\text{Zn}(\text{CH}_3\text{COOH})_2 \cdot 2\text{H}_2\text{O}$) (Sigma Aldrich, St. Louis, MS, USA, 99.0%) 0.01 M dissolved in a mixture of water and propanol with fraction volumes of 1/4 and 3/4 respectively and it was acidified with acetic acid (pH = 5) according to the experimental protocol described previously [10] [11]. Phase identification and structural analysis of the as-grown films, were carried out at room temperature by X-ray diffraction (Analytical X Pert PROMP D) with Cu-K α radiation ($\lambda = 1.54056 \text{ \AA}$), at 40 kV, 100 mA. Data for the Rietveld refinement were collected in the 2θ range 30° - 65° with a step size of 0.017°. The surface morphology was carried out by atomic force microscopy at tapping mode (AFM, VEECO digital instrument 3A). The optical measurements of ZnO thin film were performed at room temperature using a Shimadzu UV 3100 double-beam spectrophotometer in the wavelength range 300 nm - 1800 nm. The micro-Raman spectra were recorded at room temperature with a Horiba Jobin HR 800 system. A 632.8 nm line of a He-Ne laser was used for off-resonance excitation.

3. Computational Method

First-principles calculations based on Density Functional Theory (DFT) using exchange-correlation (EXC) proposed by Frisch and coauthors in 1994 were performed which described by the following equation:

$$E_{XC}^{B3LYP} = E_X^{LDA} + 0.20(E_X^{HF} - E_X^{LDA}) + 0.72(E_X^{GGA} - E_X^{LDA}) + 0.81(E_C^{GGA} - E_C^{LDA}) + E_C^{LDA} \quad (1)$$

Such hybrid functional employ the Becke functional allied to the Lee-Yang-Parr (LYP) adjustment to DFT and the Slater exchange plus Vosko, Wilk, Nusair (SVWN) to improve the formalism proposed by LYP. This calculation level was implemented in the CRYSTAL14 program package [31] [32].

An all-electron basis set of Gaussian-type functions which represent crystalline orbitals as a linear combination of Bloch functions has been adopted for oxygen and zinc. For oxygen, a [4s3p] basis as in [33], together with an extra d (exponent 0.5) was employed, resulting in a [4s3p1d] basis set. For Zn, a [6s5p2d] basis set as in [34] was used. The geometries were optimized on the basis of the convergence of analytical gradients and nuclear displacements [35]. The diagonalization was performed using a grid of k points according to the Monkhorst-Pack method [36] and the shrinking factor was set to $8 \times 8 \times 8$ corresponding to 50 independent k points in the Brillouin zone. Harmonic phonon frequencies at the center of the first Brillouin zone (Γ point) are obtained from the diagonalization of the mass-weighted Hessian matrix W of the second energy derivatives with respect to atomic displacements:

$$W_{ai,bj} = \frac{H_{ai,bj}}{\sqrt{M_a M_b}} \quad (2)$$

where atoms a and b (with atomic masses M_a and M_b) in the reference cell, 0, are displaced along the i^{th} and j^{th} Cartesian directions, respectively. The relative intensities of vibrational peaks were simulated through an analytical approach. This formalism is based on combining gradients of mono-electronic and bi-electronic integrals [37] [38] with a coupled perturbed Hartree-Fock/Kohn-Sham scheme [39] [40] for the response of the crystalline orbitals to a static electric field. The convergence threshold of the energy for the selfconsistent-field (SCF) procedure has been set to 10^{-8} hartree for structural optimizations and to 10^{-10} hartree for vibration frequency calculations [41] [42].

4. Results and Discussion

4.1. Microstructural and Rietveld Analysis

The structure refinement was carried out by the Rietveld analysis of the X-ray powder diffraction data with the FULLPROF software [43]. **Figure 1** illustrates the calculated diffraction profiles and XRD patterns of as-synthesized ZnO thin film. The recognized diffraction peaks are consistent with those of a wurtzite structure [11] [12]. It is seen that the intensity of (002) peaks was most higher than all others peaks indicating that the latter is preferentially c-axis oriented. The reliability of the calculated pattern during refinement was checked by the profile residual R_p , the weighted profile residual R_{wp} and the goodness of fit χ^2 . Refinement may be accepted for the weighted profile residual $R_{wp} < 10$ and goodness of fit $\chi^2 < 2$ [44]. On the basis of refined crystallographic data, the lattice constants, structural parameters, atomic positions and other fitting parameters of the sample are computed and given in **Table 1**. The primitive unit cell of the wurtzite structure comprising O-Zn-O bonds and contained two oxygen atoms and two zinc atoms is shown in **Figure 2**. Moreover, the arrangement of the oxygen atoms is similar to that of the zinc atoms, in which each atom is located at the center of a tetrahedron. On the other hand, it is found that the obtained value of d-spacing (2.5796 Å) for ZnO film was lower than that of the d-spacing for ZnO powder, suggesting that the film grains are compressed [45]. In addition, a study of the surface morphology of ZnO thin film was carried out by AFM (**Figure 3**). The surface of ZnO thin film appears smooth and contains smaller clusters with columnar shape and the root mean square (rms) was found to be 31.59 nm. Charpentier *et al.* reported that the column growth during the deposition of ZnO on glass substrate can be explained by the coalescence of the islands which leads to the formation of polycrystalline films by columnar growth of grains perpendicularly to the substrate plane [46]. These strongly oriented grains and broadening in experimental peaks from X-ray diffraction may be due to strain along the c-axis and the crystallite size. Assuming homogeneous strains, the crystallite size D and strain ε can be respectively estimated from the following equation:

$$\begin{cases} D = \frac{0.9\lambda}{\beta \cos \theta} \\ \varepsilon = \frac{\beta}{4 \tan \theta} \end{cases} \quad (3)$$

where β is the peak's FWHM and θ is the Bragg angle.

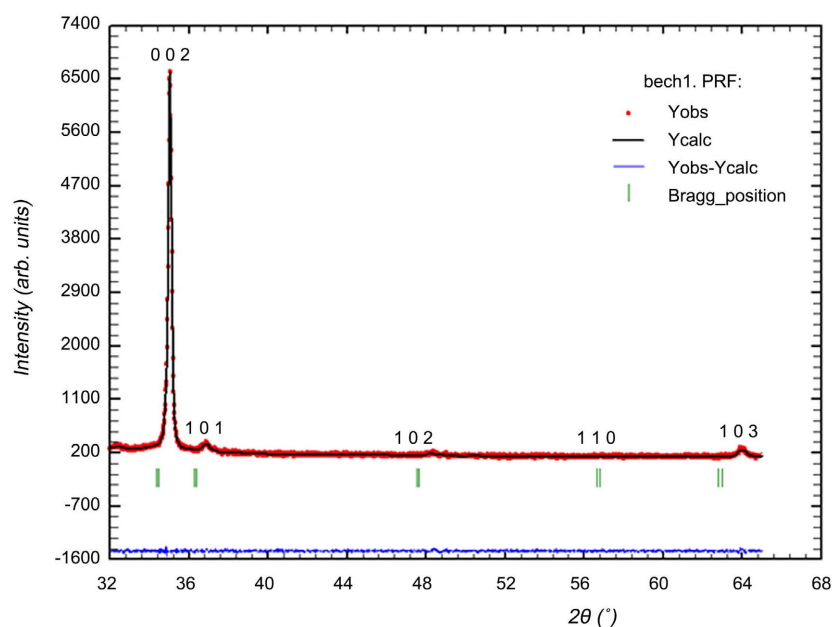


Figure 1. Rietveld plot of XRD data for ZnO thin film at room temperature. The red circles are the observed profile; the solid line is the calculated one. Tick marks below the profile indicate the position of allowed Bragg reflections.

Table 1. Refined structure parameters for ZnO thin film.

Space groupe		P 63 mc				
Unit cell parameters						
$a(\text{Å})$		3.2467				
$c(\text{Å})$		5.2151				
$V(\text{Å}^3)$		47.61				
c/a		1.6063				
Bond-length						
$d_{\text{Zn-O}}(\text{Å})$		2.6021				
Discrepancy Factor						
$R_{wp}(\%)$		2.65				
$R_p(\%)$		2.78				
$R_F(\%)$		3.89				
χ^2		1.07				
Site	Wyckoff Position	x	y	z	$B_{iso}(\text{Å}^2)$	Occ
Zn	2b	1/3	2/3	0	0.06500	0.5
O	2b	1/3	2/3	0.38224	0.07300	0.5

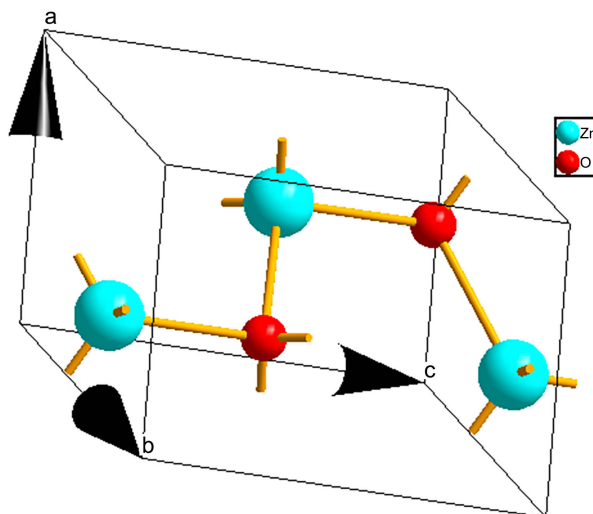


Figure 2. Crystal structure of ZnO thin film.

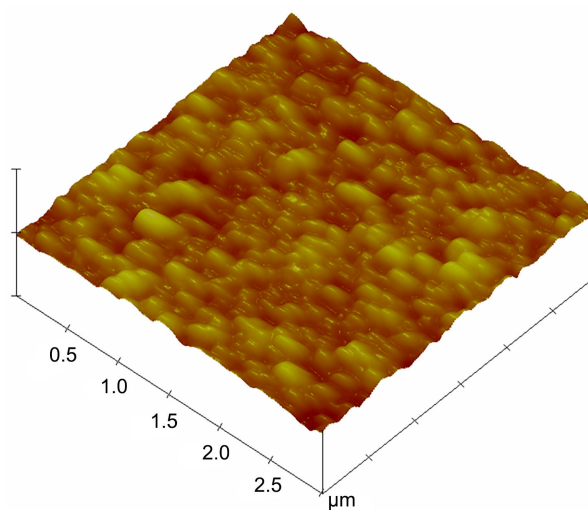


Figure 3. AFM micrograph image of ZnO thin film

The estimated value of crystallite size (D) and strain (ϵ) are respectively of the order of 37.41 nm and 6.5610^{-4} . These values are close to that previously reported [11] [12].

4.2. Structure and Optimization

The optimized geometry of ZnO bulk is obtained with DFT, employing hybrid functional B3LYP as implemented in the software CRYSTAL14. The structure of pure wurtzite-ZnO unit cell is fully optimized. The computed structural parameters and those refined from our experimental data through Rietveld analysis are presented in **Table 2**. We note that the deviation from the experimental value is only about 1%, meaning that our calculation is reasonable. Also, the values are in good agreement with other reported theoretical values in the literature [47].

Table 2. Comparison of lattice constants of ZnO thin film by Rietveld analysis obtained from XRD with geometrical optimization.

Unit cell parameters (this work)		Rietveld-analysis geometrical optimization					
$a(\text{\AA})$		3.2467			3.28223712		
$c(\text{\AA})$		5.2151			5.27346980		
$V(\text{\AA}^3)$		47.61			49.20		
c/a		1.6063			1.6066		
Site Wyckoff Position		x	y	z	x	y	z
Zn	2b	1/3	2/3	0.033	-0.33	0.0653	
O	2b	1/3	2/3	0.38224	0.33	-0.33	0.31538

4.3. Electronic Structure and Optical Properties

Figure 4 shows the transmittance and reflectance spectra of the ZnO film, which revealed an optical transmittance of above 75% in the visible range. In the range, where the absorption is high, the absorption coefficient α may be derived using the following equation [48]:

$$\begin{cases} R + T = e^{-\alpha d} \\ \alpha = \frac{1}{d} \ln \frac{(1-R)^2}{T} \end{cases} \quad (4)$$

where d is the layer thickness.

The band gap of ZnO thin film was calculated using the Tauc model by extrapolating the linear portion of the plot $(\alpha h\nu)^2$ versus incident photon energy ($h\nu$). The extrapolation of the intersection of the line with the ($h\nu$)-axis at 3.3 eV gives the value of the optical band gap (**Figure 5**). It is found that the optical absorption coefficient ($\alpha h\nu$) near the absorption edge varies exponentially with incident photon energy, which is a measure of the width of the band tails of the localized states [49] [50]. The Urbach energy which indicates the width of the band tails of the localized states has been calculated from the slope of local straight line portions in the plot of $\ln(\alpha)$ versus ($h\nu$) (inset **Figure 5**). The Urbach energy E_U value is of the order of 67.39 meV. These tails in the forbidden band affect the band gap value and govern the conduction mechanism. The obtained values of Urbach energy and band gap energy have been close to the values of our previous works in the literature [11] [12]. In addition, the optical properties are related to the band structure and density of states. The band structures of ZnO are shown in **Figure 6**. As shown in **Figure 6**, the bottom of conduction band and the top of valence band are located at the Γ point in the Brillouin zone, indicating that the ZnO is a direct band gap semiconductor. The calculated band gap is 3.35 eV, which is close to the optical band gap estimated from the ultraviolet-visible transmittance and reflectance spectra of the ZnO films (3.3 eV). It seems that the B3LYP functional provides a reliable band gap for ZnO. Other theoretical calculations cover a wide spectrum varying from 0.23 eV to 4.23 eV, mostly disagree with experimental measurements [51] [52]. These

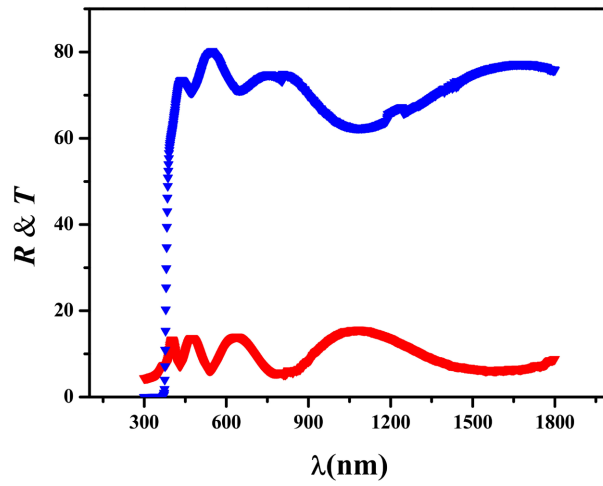


Figure 4. Transmission (T) and reflection (R) spectra of ZnO thin film.

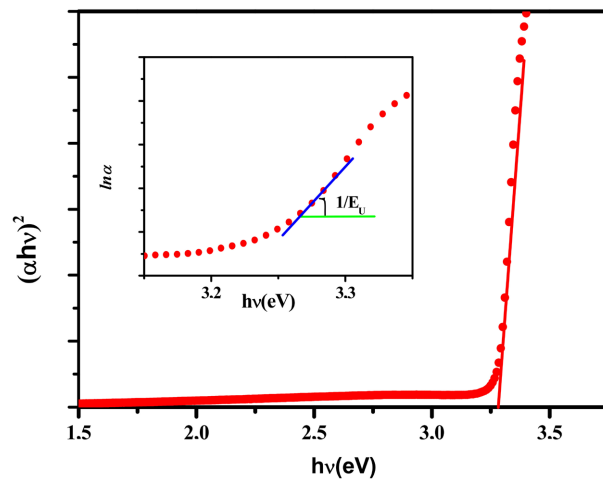


Figure 5. Plot of $(\alpha hv)^2$ versus (hv) of ZnO thin film.

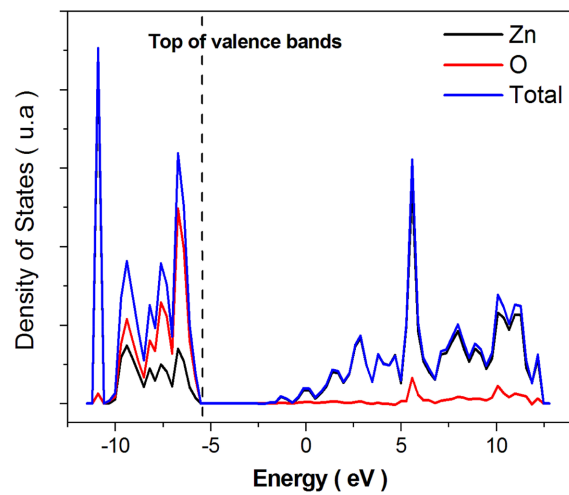


Figure 6. Density of states of ZnO materials obtained through of DFT/B3LYP calculation level.

strong difference in calculation mainly due to the choice of the basis set describing the ground state [20]. It is found that the basis set which include the d orbitals is expected to be an optimal basis set. Defects induced by structural disorder may lead to the appearance of localized states in the band gap, called band tails which can affect the Fermi level and this latter may lead to further discrepancies between observed and computed band gaps [5] [53]. It should be noted that the discrepancy between the computed and observed band gaps is of the same order of magnitude as the Urbach energy. The simulated Density of states (DOS) of wurtzite ZnO is shown in **Figure 7** for the energy range -10 eV to $+10$ eV. The DOS reveals that the valence band is mainly formed by Zn 3d states and O 2p states, whereas the conduction band is essentially occupied by Zn 4s states. A similar density of states has been obtained by Chuanhui *et al.*, while the gap is smaller [51]. Moreover, Zhi *et al.* reported that the strong interaction between O 2p and Zn 3d bands may lead to the observed difference between calculated band gap and the experimental one [16]. The band gap provides information on the electronic structure of the compound for the possible application in optoelectronic devices. IR and Raman spectroscopy are useful for the interpretation of the structure and bonding strength, and can provide a detailed understanding. Serrano *et al.* indicated that the discrepancy between the calculated and measured phonon modes is primarily related to the underestimated band gap [54].

4.4. Phonon Properties

According to the group theory, wurtzite structured ZnO belongs to the space group $P6_3mc$ with unit of four atoms in the unit cell. At the Γ -point of the Brillouin zone, group theory predicts the following irreducible representations of the lattice optical phonons:

$$\Gamma_{Opt} = 1A_1 + 2B_1 + 1E_1 + 2E_2 \quad (5)$$

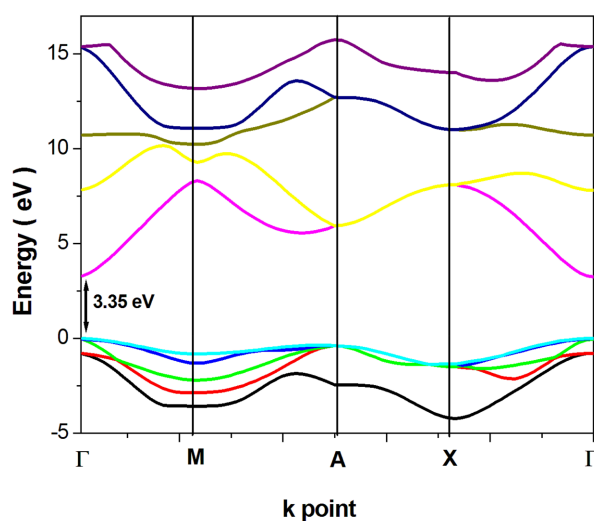


Figure 7. The band structure of ZnO materials obtained through of DFT/B3LYP calculation level.

where B_1 modes are IR and Raman inactive and the two non-polar E_2 modes are only Raman active. In addition, the polar A_1 and E_1 modes are IR and Raman active, and therefore they split into longitudinal and transverse optical phonons (LO and TO).

The experimental Raman spectra with the corresponding theoretically simulated one are shown in **Figure 8**. All the calculated frequencies and their assignments are presented in **Table 3**. The experimental Raman spectrum of the ZnO thin film recorded at room temperature exhibits two prominent peaks at 110 and 450 cm^{-1} assigned to E_2 (high) and E_2 (low) Raman active mode in the wurtzite crystal structure [55]. A similar result has been observed in ZnO bulk and thin film [56]. The two non-polar E_2 (high) and E_2 (low) modes are associated with the vibration of oxygen (O) atoms and zinc (Zn) sublattice, respectively [57]. Thus, the E_2 low mode corresponds to the vibration of the heavy zinc sublattice, while the E_2 (high) mode is associated with the vibration of the lighter oxygen sublattice. In addition, the strong E_2 (high) mode is an indication on the good crystallinity [58]. The DFT predicted Raman spectrum of ZnO exhibits three main intense bands located at 100 cm^{-1} , 380 cm^{-1} and 425 cm^{-1} assigned to E_2 (high), A_1 and E_2 (low) modes, respectively. The very weak band at 403 cm^{-1} is assigned to E_1 mode. From these data, we remark that the agreement with our experimental results is quite satisfactory for E_2 high mode, whereas the experimental frequency of the E_2 Low mode is slightly lower than the simulated one. This discrepancy may be caused by structural defects. In fact, Wrzesinski *et al.* reported that tensile stress in the wurtzite-structure affects the E_2 phonon wave-number [59]. Furthermore, the compressive strain in the films that caused the Raman peaks shift was consistent with that obtained from the XRD result [57]. The calculated IR active optical phonon modes of wurtzite ZnO shows two peaks at wavelengths in the range from 0 to 900 cm^{-1} (**Figure 9**). The most characteristic bands are at 380 and 403 cm^{-1} . These peaks are attributed to TO phonons of A_1 and E_1 modes [60]. The most intense peak at 403 cm^{-1} is assigned to Zn-O stretching vibrations [61]. Moreover, $E_1(\text{TO})$ and $A_1(\text{TO})$ modes reflect the strength of the polar lattice bonds [62].

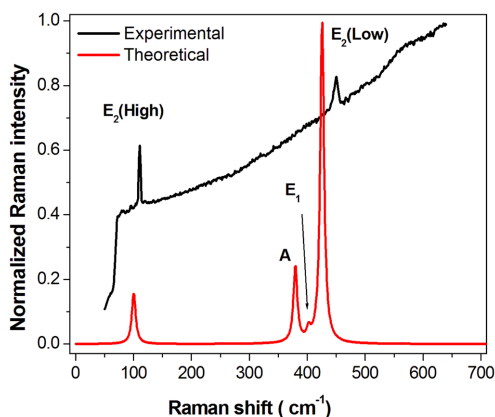


Figure 8. Theoretical and experimental Raman spectrum of ZnO thin film.

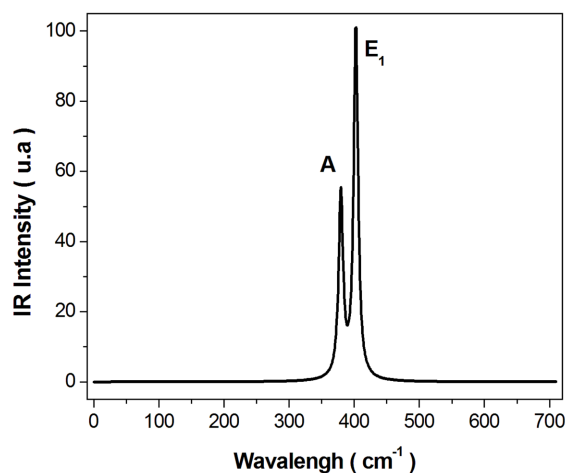


Figure 9. Theoretical IR spectrum of ZnO materials obtained through of DFT/B3LYP calculation level.

Table 3. Detailed assignments of theoretically computed IR and Raman vibrations of ZnO.

(cm ⁻¹) Sym.	IR IR intensity	Raman	Raman intensity	
100.3970	E2	I	A	156.94
379.5879	A1	A 665.80	A	236.60
402.5345	E1	A 1267.93	A	32.08
425.8058	E2	I	A	1000.00

5. Conclusion

In summary, this work deals with the X-ray diffraction, UV-Vis spectrophotometry, IR and Raman spectral investigations of sprayed ZnO thin film supported by first principle *ab initio* DFT calculations using hybrid (B3LYP) as exchange and correlation functional. Band structure and DOS of bulk wurtzite ZnO have been calculated. ZnO thin film has hexagonal wurtzite structure with a smooth surface and a growth in a preferred orientation along the direction (002). The optimized structural parameters of wurtzite structure of ZnO were found to be close to the experimental data. Our calculated band gap of 3.35 eV is in excellent agreement with the measured value of 3.3 eV. The simulated Raman spectra of ZnO were also similar to experimental data. The above results show the ability of the DFT to accurately describe and predict the electronic and vibrational properties of semiconductors.

Conflicts of Interest

The authors declare no conflicts of interest regarding the publication of this paper.

References

- [1] Aoki, T. and Hatanaka, Y. (2000) ZnO Diode Fabricated by Excimer-Laser Doping.

- Applied Physics Letters*, **76**, 3257-3258. <https://doi.org/10.1063/1.126599>
- [2] Lupan, O., Emelchenko, G.A., Ursaki, V.V., Chai, G., Redkin, A.N., Gruzintsev, A.N., Tiginyanu, I.M., Chow, L., Ono, L.K., Cuenya, B.R., Heinrich, H. and Yakimov, E.E. (2010) Synthesis and Characterization of ZnO Nanowires for Nanosensor Applications. *Materials Research Bulletin*, **45**, 1026-1032. <https://doi.org/10.1016/j.materresbull.2010.03.027>
- [3] Zhang, Q., Dandeneau, C.S., Zhou, X. and Cao, G. (2009) ZnO Nanostructures for Dye-Sensitized Solar Cells. *Advanced Materials*, **21**, 4087-4108. <https://doi.org/10.1002/adma.200803827>
- [4] Norton, D.P., Heo, Y.W., Ivill, M.P., Ip, K., Pearton, S.J., Chisholm, M.F. and Steiner, T. (2004) ZnO: Growth, Doping & Processing. *Materials Today*, **7**, 34-40. [https://doi.org/10.1016/S1369-7021\(04\)00287-1](https://doi.org/10.1016/S1369-7021(04)00287-1)
- [5] Janotti, A. and Van de Walle, C.G. (2009) Fundamentals of Zinc Oxide as a Semiconductor. *Reports on Progress in Physics*, **72**, 126501-126530. <https://doi.org/10.1088/0034-4885/72/12/126501>
- [6] Lacerda, L.H.S. and Lazaro, S.R.L. (2016) Ba-Doped ZnO Materials: A DFT Simulation to Investigate the Doping Effect on Ferroelectricity. *Química Nova*, **39**, 261-266. <https://doi.org/10.5935/0100-4042.20160023>
- [7] Reza, E., Reza, G.M. and Hossein, A. (2014) Sol-Gel Derived Al and Ga Co-Doped ZnO Thin Films: An Optoelectronic Study. *Applied Surface Science*, **290**, 252-259. <https://doi.org/10.1016/j.apsusc.2013.11.062>
- [8] Qasem, A.D., Saleem, G.R., Zain, H.Y. and Mohammed, A.G. (2013) Crystalline Nanostructured Cu Doped ZnO Thin Films Grown at Room Temperature by Pulsed Laser Deposition Technique and Their Characterization. *Applied Surface Science*, **270**, 104-108. <https://doi.org/10.1016/j.apsusc.2012.12.126>
- [9] Young, M.T. and Hee, C.M. (2013) Optical and Electrical Properties of Mg-Doped Zinc Tin Oxide Films Prepared by Radio Frequency Magnetron Sputtering. *Applied Surface Science*, **286**, 131-136. <https://doi.org/10.1016/j.apsusc.2013.09.035>
- [10] Li, X., Asher, S.E., Limpijumnong, S., Keyes, B.M., Perkins, C.L., Barnes, T.M., Moutinho, H.R., Luther, J.M., Zhang, S.B., Wei, S.H. and Coutts, T.J. (2006) Impurity Effects in ZnO and Nitrogen-Doped ZnO Thin Films Fabricated by MOCVD. *Journal of Crystal Growth*, **287**, 94-100. <https://doi.org/10.1016/j.jcrysgro.2005.10.050>
- [11] Boukhachem, A., Ouni, B., Karyauoi, M., Madani, A., Chtourou, R. and Amlouk, M. (2012) Structural, Opto-Thermal and Electrical Properties of ZnO:Mo Sprayed Thin Films. *Materials Science in Semiconductor Processing*, **15**, 282-292. <https://doi.org/10.1016/j.mssp.2012.02.014>
- [12] Mhamdi, A., Ouni, B., Amlouk, A., Boubaker, K. and Amlouk, M. (2014) Study of Nickel Doping Effects on Structural, Electrical and Optical Properties of Sprayed ZnO Semiconductor Layers. *Journal of Alloys and Compounds*, **582**, 810-822. <https://doi.org/10.1016/j.jallcom.2013.08.080>
- [13] Abd-Lefdil, M., Douayar, A., Belayachi, A., Reshak, A.H., Fedorchuk, A.O., Pramodini, S., Poornesh, P., Nagaraja, K.K. and Nagaraja, H.S. (2014) Third Harmonic Generation Process in Al Doped ZnO Thin Films. *Journal of Alloys and Compounds*, **584**, 7-12. <https://doi.org/10.1016/j.jallcom.2013.08.134>
- [14] Ilican, S., Caglar, Y., Caglar, M. and Yakuphanoglu, F. (2006) Electrical Conductivity, Optical and Structural Properties of Indium-Doped ZnO Nanofiber Thin Film Deposited by Spray Pyrolysis Method. *Physica E: Low-Dimensional Systems and Nanostructures*, **35**, 131-138. <https://doi.org/10.1016/j.physe.2006.07.009>

- [15] Mariappan, R., Ponnuswamy, V., Suresh, P., Suresh, R., Ragavendar, M. and Chandra, B.A. (2014) Nanostructured $Ce_xZn_{1-x}O$ Thin Films: Influence of Ce Doping on the Structural, Optical and Electrical Properties. *Journal of Alloys and Compounds*, **588**, 170-176. <https://doi.org/10.1016/j.jallcom.2013.10.210>
- [16] Yu, Z.G., Gong, H. and Wu, P. (2006) Lattice Dynamics and Electrical Properties of Wurtzite ZnO Determined by a Density Functional Theory Method. *Journal of Crystal Growth*, **287**, 199-203. <https://doi.org/10.1016/j.jcrysgro.2005.10.067>
- [17] Bovhyra, R., Popovych, D., Bovgyra, O. and Serednytski, A. (2017) *Ab Initio* Study of Structural and Electronic Properties of $(ZnO)_n$ "Magical" Nanoclusters $n = (34, 60)$. *Nanoscale Research Letters*, **12**, 76-82. <https://doi.org/10.1186/s11671-017-1848-8>
- [18] Charifi, Z., Baaziz, H. and Reshak, A.H. (2007) *Ab-Initio* Investigation of Structural, Electronic and Optical Properties for Three Phases of ZnO Compound. *Physica Status Solidi*, **244**, 3154-3167. <https://doi.org/10.1002/pssb.200642471>
- [19] John, R. and Padmavathi, S. (2016) *Ab Initio* Calculations on Structural, Electronic and Optical Properties of ZnO in Wurtzite Phase. *Crystal Structure Theory and Applications*, **5**, 24-41. <http://www.scirp.org/journal/csta>
<https://doi.org/10.4236/csta.2016.52003>
- [20] Franklin, L., Ekuma, C.E., Zhao, G.L. and Bagayoko, D. (2013) Density Functional Theory Description of Electronic Properties of Wurtzite Zinc Oxide. *Journal of Physics and Chemistry of Solids*, **74**, 729-736. <https://doi.org/10.1016/j.jpics.2013.01.013>
- [21] Calzolari, A. and Nardelli, M.B. (2013) Dielectric Properties and Raman Spectra of ZnO from a First Principles Finite-Differences/Finite-Fields Approach. *Scientific Reports*, **3**, Article No. 2999. <https://doi.org/10.1038/srep02999>
- [22] Bernasconi, L., Tomić, S., Ferrero, M., Rérat, M., Orlando, R., Dovesi, R. and Harrison, N.M. (2011) First-Principles Optical Response of Semiconductors and Oxide Materials. *Physical Review B*, **83**, 195325-195332. <https://doi.org/10.1103/PhysRevB.83.195325>
- [23] Samanta, K., Dussan, S., Katiyar, R.S. and Bhattacharya, P. (2007) Structural and Optical Properties of Nanocrystalline $Zn_{1-x}Mn_xO$. *Applied Physics Letters*, **90**, 261903-261906. <https://doi.org/10.1063/1.2751593>
- [24] Brittman, S., Adhyaksa, G.W.P. and Garnett, E.C. (2015) The Expanding World of Hybrid Perovskites: Materials Properties and Emerging Applications. *MRS Communications*, **5**, 7-26. <https://doi.org/10.1557/mrc.2015.6>
- [25] Damen, T., Porto, S. and Tell, B. (1966) Raman Effect in Zinc Oxide. *Physical Review*, **142**, 570-574. <https://doi.org/10.1103/PhysRev.142.570>
- [26] Cheng, A., Tzeng, Y., Xu, H., Alur, S., Wang, Y., Park, M., Wu, T., Shannon, C., Kim, D. and Wang, D. (2009) Raman Analysis of Longitudinal Optical Phonon-Plasmon Coupled Modes of Aligned ZnO Nanorods. *Journal of Applied Physics*, **105**, Article ID: 073104. <https://doi.org/10.1063/1.3093877>
- [27] Serrano, J., Widulle, F., Romero, A.H., Rubio, A., et al. (2003) Dependence of Phonon Widths on Pressure and Isotopic Mass: ZnO. *Physica Status Solidi (b)*, **235**, 260-266. <https://doi.org/10.1002/pssb.200301566>
- [28] McCluskey, M.D. and Jokela, S.J. (2009) Defects in ZnO. *Journal of Applied Physics*, **106**, 71101-71104. <https://doi.org/10.1063/1.3216464>
- [29] Cheng, B., Sun, W., Jiao, J., Tian, B., Xiao, Y. and Lei, S. (2010) Disorder-Induced Raman Scattering Effects in One-Dimensional ZnO Nanostructures by Incorporation and Anisotropic Distribution of Dy and Li Codopants. *Journal of Raman Spectroscopy*, **41**, 1221-1226. <https://doi.org/10.1002/jrs.2590>

- [30] Raymand, D., Jacobsson, T.J., Hermansson, K. and Edvinsson, T. (2012) Investigation of Vibrational Modes and Phonon Density of States in ZnO Quantum Dots. *The Journal of Physical Chemistry C*, **116**, 6893-6901. <https://doi.org/10.1021/jp300985k>
- [31] Becke, A.D. (1998) A New Inhomogeneity Parameter in Density-Functional Theory. *The Journal of Chemical Physics*, **109**, 2092-2099. <https://doi.org/10.1063/1.476722>
- [32] Dovesi, R., Saunders, V.R., Roetti, C., Orlando, R., Zicovich-Wilson, C.M., Pascale, F., Civalieri, B., Doll, K., Harrison, N.M., Bush, I.J., Ph D'Arco, L., Llunell, M., Causà, M., Noël, Y., Maschio, L., Erba, A., Rerat, M. and Casassa, S. (2014) CRYSTAL14 User's Manual. University of Torino, Torino, 382. <http://www.crystal.unito.it>
- [33] Towler, M.D., Allan, N.L., Harrison, N.M., Saunders, V.R., Mackrodt, W.C. and Aprà, E. (1994) *Ab Initio* Study of MnO and NiO. *Physical Review B*, **50**, 5041-5054. <https://doi.org/10.1103/PhysRevB.50.5041>
- [34] Jaffe, J.E. and Hess, A.C. (1993) Hartree-Fock Study of Phase Changes in ZnO at High Pressure. *Physical Review B*, **48**, 7903-7909. <https://doi.org/10.1103/PhysRevB.48.7903>
- [35] Doll, K. (2001) Implementation of Analytical Hartree-Fock Gradients for Periodic Systems. *Computer Physics Communications*, **137**, 74-88. [https://doi.org/10.1016/S0010-4655\(01\)00172-2](https://doi.org/10.1016/S0010-4655(01)00172-2)
- [36] Monkhorst, H.J. and Pack, J.D. (1976) Special Points for Brillouin-Zone Integrations. *Physical Review B*, **13**, 5188-5192. <https://doi.org/10.1103/PhysRevB.13.5188>
- [37] Maschio, L., Kirtman, B., Salustro, S., Zicovich-Wilson, C.M., Orlando, R. and Dovesi, R. (2013) Raman Spectrum of Pyrope Garnet. A Quantum Mechanical Simulation of Frequencies, Intensities, and Isotope Shifts. *The Journal of Physical Chemistry A*, **117**, 11464-11471. <https://doi.org/10.1021/jp4099446>
- [38] Ferrero, M., Rerat, M., Kirtman, B. and Dovesi, R. (2008) Calculation of First and Second Static Hyperpolarizabilities of One- to Three-Dimensional Periodic Compounds. Implementation in the CRYSTAL Code. *The Journal of Chemical Physics*, **129**, Article ID: 244110. <https://doi.org/10.1063/1.3043366>
- [39] Maschio, L., Kirtman, B., Rerat, M., Orlando, R. and Dovesi, R. (2013) *Ab Initio* Analytical Raman Intensities for Periodic Systems through a Coupled Perturbed Hartree-Fock/Kohn-Sham Method in an Atomic Orbital Basis. I. Theory. *The Journal of Chemical Physics*, **139**, 164101-164124. <https://doi.org/10.1063/1.4824442>
- [40] Ferrari, A.M., Valenzano, L., Meyer, A., Orlando, R. and Dovesi, R. (2009) Quantum-Mechanical *Ab Initio* Simulation of the Raman and IR Spectra of Fe₃Al₂Si₃O₁₂ Almandine. *The Journal of Physical Chemistry A*, **113**, 11289-11294. <https://doi.org/10.1021/jp901993e>
- [41] Doll, K., Saunders, V.R. and Harrison, N.M. (2001) Analytical Hartree-Fock Gradients for Periodic Systems. *International Journal of Quantum Chemistry*, **82**, 1-13. [https://doi.org/10.1002/1097-461X\(2001\)82:1<1::AID-QUA1017>3.0.CO;2-W](https://doi.org/10.1002/1097-461X(2001)82:1<1::AID-QUA1017>3.0.CO;2-W)
- [42] Doll, K., Dovesi, R. and Orlando, R. (2004) Analytical Hartree-Fock Gradients with Respect to the Cell Parameter for Systems Periodic in Three Dimensions. *Theoretical Chemistry Accounts*, **112**, 394-402. <https://doi.org/10.1007/s00214-004-0595-y>
- [43] Rietveld, H.M. (1969) A Profile Refinement Method for Nuclear and Magnetic Structures. *Journal of Applied Crystallography*, **2**, 65-71. <https://doi.org/10.1107/S0021889869006558>
- [44] Guinebretière, R. (2007) X-Ray Diffraction by Polycrystalline Materials. ISTE Ltd., London. <https://doi.org/10.1002/9780470612408>

- [45] Ismail, A. and Abdullah, M.J. (2013) The Structural and Optical Properties of ZnO Thin Films Prepared at Different RF Sputtering Power. *Journal of King Saud University—Science*, **25**, 209-215. <https://doi.org/10.1016/j.jksus.2012.12.004>
- [46] Charpentier, C., Prod'homme, P., Maurin, I., Chaigneau, M. and Roca iCabarrocas, P. (2011) X-Ray Diffraction and Raman Spectroscopy for a Better Understanding of ZnO:Al Growth Process. *EPJ Photovoltaics*, **2**, 25002-25010. <https://doi.org/10.1051/epjpv/2011026>
- [47] Harun, K., Mansor, N., Ahmad, Z.A. and Mohamad, A.A. (2016) Electronic Properties of ZnO Nanoparticles Synthesized by Sol-Gel Method: A LDA+U Calculation and Experimental Study. *Procedia Chemistry*, **19**, 125-132. <https://doi.org/10.1016/j.proche.2016.03.125>
- [48] Ouni, B., Zouini, M., Lakhdar, M.H., Larbi, T., Dimassi, W. and Amlouk, M. (2015) Preparation and Characterization of the Rod-Shaped Stibnite. *Materials Research Bulletin*, **67**, 191-195. <https://doi.org/10.1016/j.materresbull.2015.03.003>
- [49] Boubaker, K. (2011) Atomic Structures beyond the Spherical Approximation along with PNC as Conjectured Explanations to Urbach Tailing in Neutral Isolated Ytterbium. *The European Physical Journal B*, **84**, 235-239. <https://doi.org/10.1140/epjb/e2011-20614-y>
- [50] Boubaker, K. (2013) A Support to the Lattice Compatibility Theory: Nanoscale Patterns of Manganese-Doped Lattices in Terms of the Urbach Energy and Faraday Effect. *Mendeleev Communications*, **23**, 160-162. <https://doi.org/10.1016/j.mencom.2013.05.014>
- [51] Xia, C., Wang, F. and Hu, C. (2014) Theoretical and Experimental Studies on Electronic Structure and Optical Properties of Cu-Doped ZnO. *Journal of Alloys and Compounds*, **589**, 604-608. <https://doi.org/10.1016/j.jallcom.2013.11.066>
- [52] Alkahtani, E.A., Merad, A.E., Boufatah, M.R. and Benosman, A. (2017) DFT Investigation of Structural, Electronic and Optical Properties of Pure and Er-Doped ZnO: Modified Becke-Johnson Exchange Potential. *Optik*, **128**, 274-280. <https://doi.org/10.1016/j.ijleo.2016.10.032>
- [53] Muscat, J., Wander, A. and Harrison, N.M. (2001) On the Prediction of Band Gaps from Hybrid Functional Theory. *Chemical Physics Letters*, **342**, 397-401. [https://doi.org/10.1016/S0009-2614\(01\)00616-9](https://doi.org/10.1016/S0009-2614(01)00616-9)
- [54] Serrano, J., Romero, A., Manjón, F., Lauck, R., Cardona, M. and Rubio, A. (2004) Pressure Dependence of the Lattice Dynamics of ZnO: An *Ab Initio* Approach. *Physical Review B*, **69**, 94306-94320. <https://doi.org/10.1103/PhysRevB.69.094306>
- [55] Cuscó, R., Alarcón-Lladó, E., Ibáñez, J., Artús, L., Jiménez, J., Wang, B. and Callahan, M. (2007) Temperature Dependence of Raman Scattering in ZnO. *Physical Review B*, **75**, 165202-165213. <https://doi.org/10.1103/PhysRevB.75.165202>
- [56] Yahia, S.B., Znaidi, L., Kanaev, A. and Petitet, J.P. (2008) Raman Study of Oriented ZnO Thin Films Deposited by Sol-Gel Method. *Spectrochimica Acta Part A*, **71**, 1234-1238. <https://doi.org/10.1016/j.saa.2008.03.032>
- [57] Shkir, M., Chandekar, K.V., Alshehri, B.M., Khan, A., AlFaify, S. and Hamdy, M.S. (2020) A Remarkable Enhancement in Photocatalytic Activity of Facilely Synthesized Terbium@Zinc Oxide Nanoparticles by Flash Combustion Route for Optoelectronic Applications. *Applied Nanoscience*, **10**, 1811-1823. <https://doi.org/10.1007/s13204-019-01236-6>
- [58] Thangavel, R., Moirangthem, R.S., Lee, W.S., Chang, Y.C., Wei, P.K. and Kumar, J. (2010) Cesium Doped and Undoped ZnO Nanocrystalline Thin Films: A Comparative Study of Structural and Micro-Raman Investigation of Optical Phonons. *Jour-*

- nal of Raman Spectroscopy*, **41**, 1594-1600. <https://doi.org/10.1002/jrs.2599>
- [59] Wrzesinski, J. and Fröhlich, D. (1997) Two-Photon and Three-Photon Spectroscopy of ZnO under Uniaxial Stress. *Physical Review B*, **56**, 13087-13093. <https://doi.org/10.1103/PhysRevB.56.13087>
- [60] Pandiyarajan, T. and Karthikeyan, B. (2012) Cr Doping Induced Structural, Phonon and Excitonic Properties of ZnO Nanoparticles. *Journal of Nanoparticle Research*, **14**, 647-656. <https://doi.org/10.1007/s11051-011-0647-x>
- [61] Khan, Z.R., Khan, M.S., Zulfequar, M. and Shahid Khan, M. (2011) Optical and Structural Properties of ZnO Thin Films Fabricated by Sol-Gel Method. *Materials Sciences and Applications*, **2**, 340-345. <https://doi.org/10.4236/msa.2011.25044>
- [62] Ashkenov, N., Mbenkum, B.N., Bundesmann, C., Riede, V., Lorenz, M., Spemann, D., Kaidashev, E.M., Kasic, A., Schubert, M., Grundmann, M., Wagner, G., Neumann, H., Darakchieva, V., Arwin, H. and Monemar, B. (2003) Infrared Dielectric Functions and Phonon Modes of High-Quality ZnO Films. *Journal of Applied Physics*, **93**, 126-133. <https://doi.org/10.1063/1.1526935>